University of Cologne

Practical Course M

Computational Physics

Tensor Networks

Sangeet Srinivasan

Tutor: Guo-Yi Zhu

September 27, 2023

Contents

Warm-Up

For the warm-up tasks we decompose a random 20 site ITensor object [2] of spin$-1/2$ states into a normalised Matrix Product State (MPS). We then calculate and plot the entanglement entropy of this state across different partition sizes and also the entanglement spectrum, which correspond to the singular values of the Schmidt decomposition of the state. We find that the entanglement

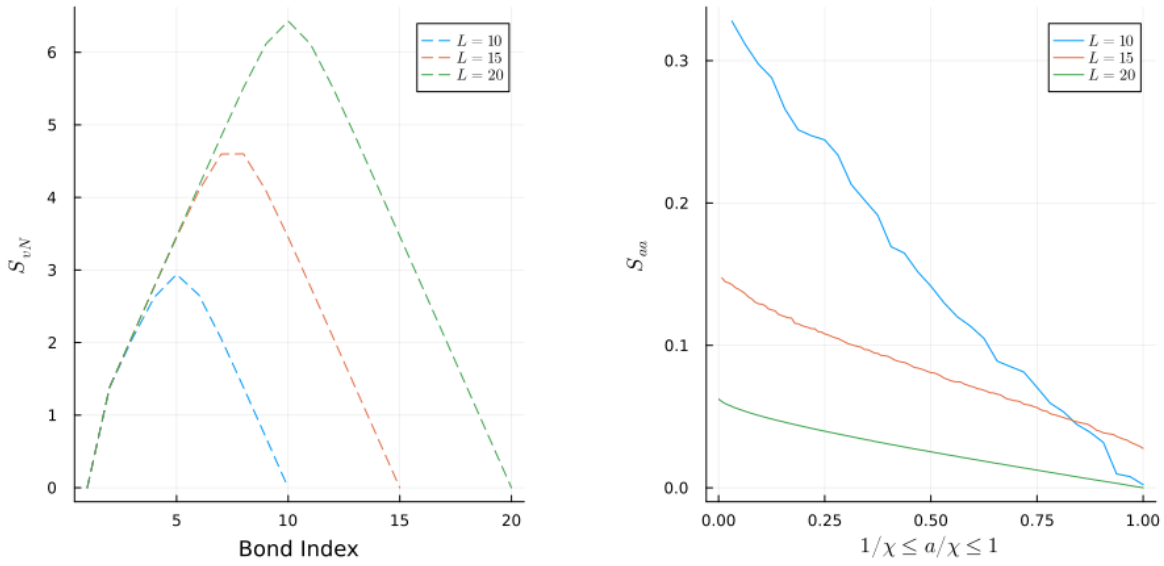

Figure 1: (Left) Entanglement Entropies vs Bond Index, (Right) Entanglement Spectrum vs Relative Bond Dimension

entropies symmetric across the bond index at the center for all sizes. In other words, the entanglement entropy is symmetric about the half-chain length. This is typical for highly entangled states which follow a volume law. As a result of the highly entangled nature of the random MPS, we also observe a slowly and monotonically decreasing entanglement spectrum. The slope of this decrease appears to decrease with system size.

Chapter 1

Transverse Field Ising Model (TFIM)

1.1 Long-Range Order

Using the DMRG algorithm [2], we are able to compute the ground state associated to the TFIM Hamiltonian given by,

$$H = -\sum_{i=1}^{L-1} S_i^z S_{i+1}^z - g \sum_{i=1}^{L} S_i^x \tag{1.1}$$

Using the ground states $|\psi_0\rangle$ associated to various fields g, we are able to observe how the squared magnetisation, i.e, $\langle M_z^2 \rangle = \langle \psi_0 | S_z^2 | \psi_0 \rangle$ changes with respect to g. Here S_z is the mean spin operator of the lattice. We choose our system size to be 80.

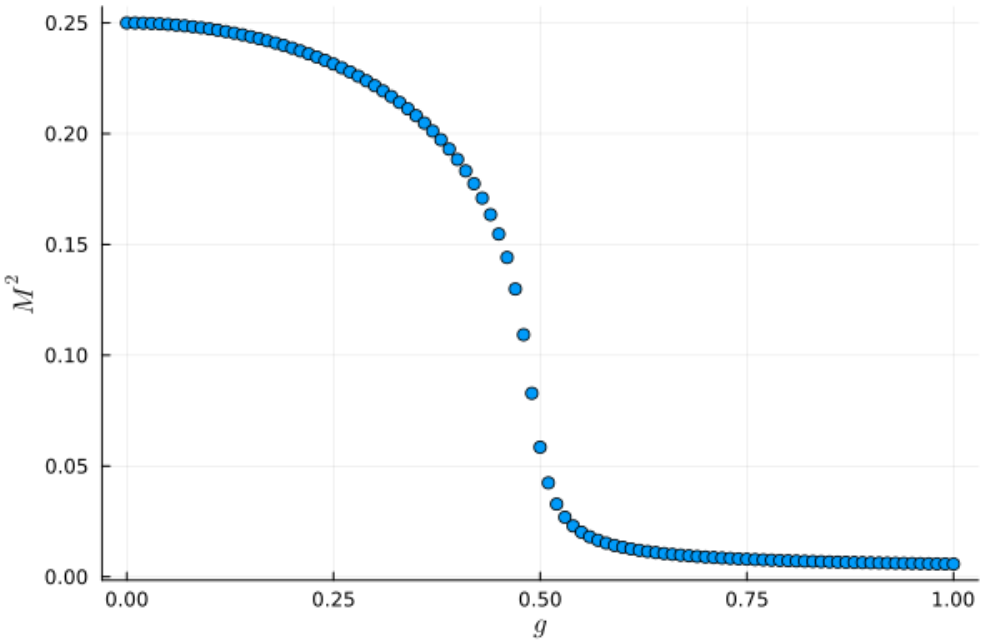

Figure 1.1: Magnetisation vs Transverse Field

Immediately we see (fig 1.1) that the $\langle M_z^2 \rangle$ starts with an ordered phase as it monotinically collapses to zero at around $g \approx 0.5$. Since we suspect this to be the critical value, we can verify this by

computing the so-called *binder cumulant* given by,

$$U_L = 1 - \frac{\langle M_z^4 \rangle_L}{3 \langle M_z^2 \rangle_L}, \tag{1.2}$$

where, L is the system size. We plot these (fig 1.2a) for different system sizes $L \in \{60, 65, 70, 75, 80\}$ and observe that all the curves share a unique crossing point at $g_c = 0.5$. Performing a finite-size scaling collapse (fig 1.2b), we obtain the order parameter $\nu \approx 1.05$ which is close to the theoretical value of $\nu = 1$. The error may be attributed to the chosen parameters for the DMRG sweeps.

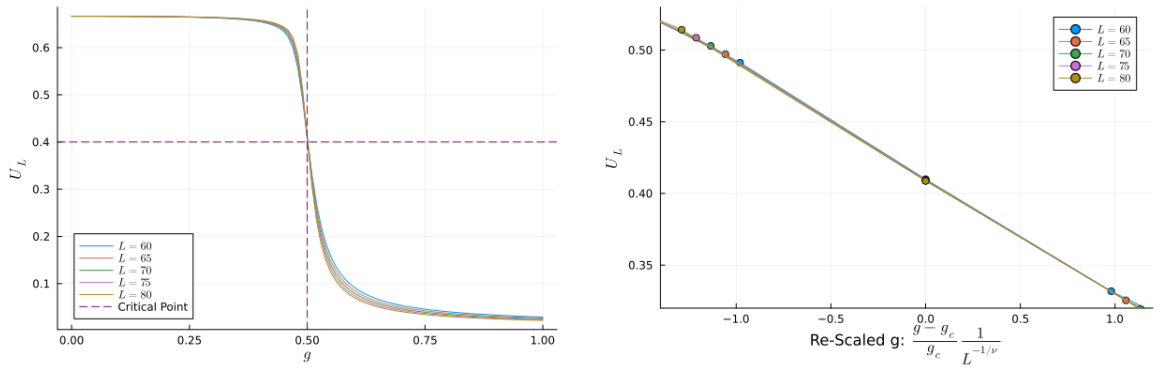

(a) $\langle M_z^2 \rangle$ vs Transverse Field

(b) Binder Cumulant vs Transverse Field

Figure 1.2: Determining the Critical Point

1.2 Energy Gaps

Using the DMRG algorithm, we are also able to compute excited states and the energies associated to a state. We use this to determine the energy gap between the ground and excited state. This is shown in figure 1.3a We note that the states are degenerate below the critical point and thus the energy gap vanishes. Beyond this, the energy gap is seen to be monotonically increasing. Performing a scaling collapse on the energy gaps yields a dynamical critical exponent $z \approx 0.99$, which is very close to the literature value of $z = 1$.

1.3 Central Charge

The Half-chain von-Neumann entropy at the critical point for a given system size is [3],

$$S_L^{vN}(l) = \frac{c}{6} \ln L + \mathcal{O}(1), \tag{1.3}$$

where. In fig 1.3b, we plot the entropies at the critical point against $\log L$. The fit gives us a value of $c \approx 0.48$ which is very close to the literature value of $c = 0.5$.

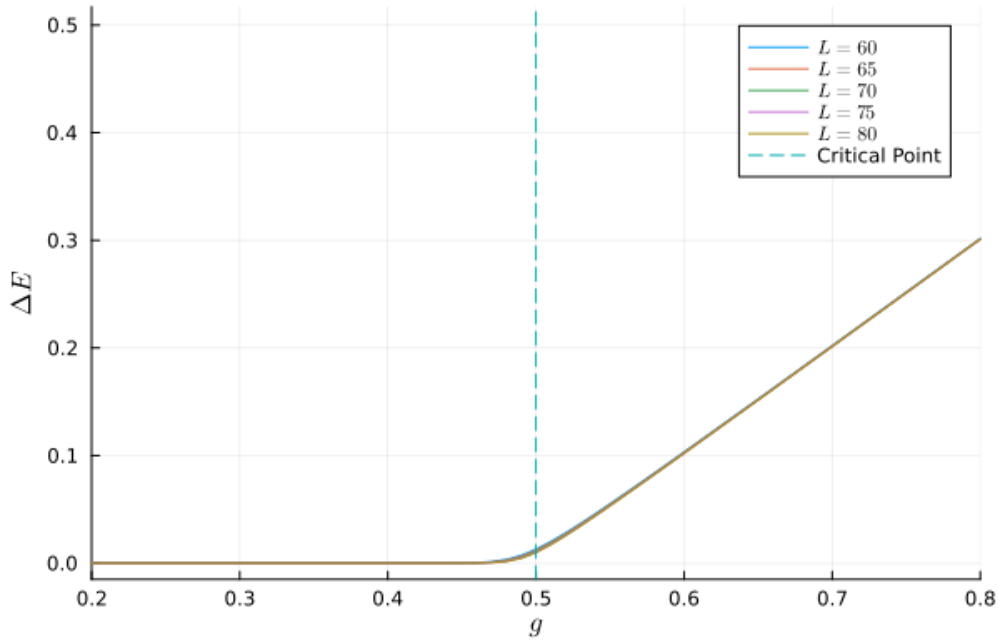

(a) Energy Gaps between ground and first excited state as a function of g.

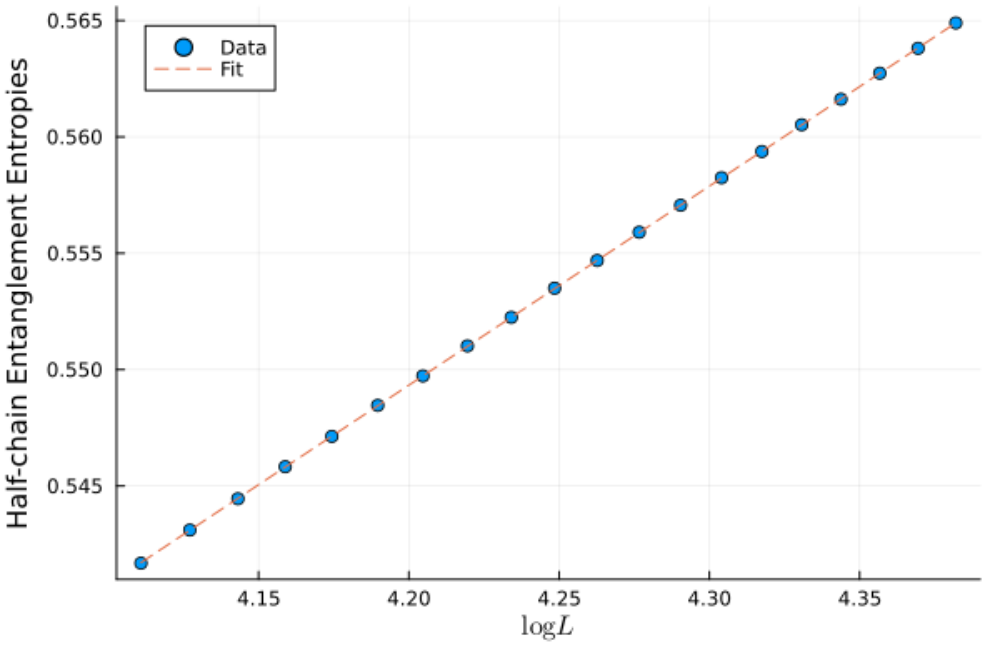

(b) Entanglement Entropy at $g_c = 0.5$.

Figure 1.3: Critical Behaviour

Chapter 2

Bilinear Biquadratic Chain (BBC)

2.1 AKLT Ground State

Using DMRG, we compute the ground state of a BBC spin-1 Hamiltonian given by,

$$H = \cos\theta \sum_{i=1}^{L-1} S_i^z S_{i+1}^z - \sin\theta \sum_{i=1}^{L-1} \left(S_i^z S_{i+1}^z\right)^2, \tag{2.1}$$

for $\theta = \arctan 1/3$, which corresponds to the so-called AKLT point. This yields an MPS of 3 dimensional sites and 2 dimensional bonds. This agrees with the theoretical expectation that the local spin-1 can be seen as a triplet of a pair of fictitious spin$-1/2$ states.

2.2 String Correlator

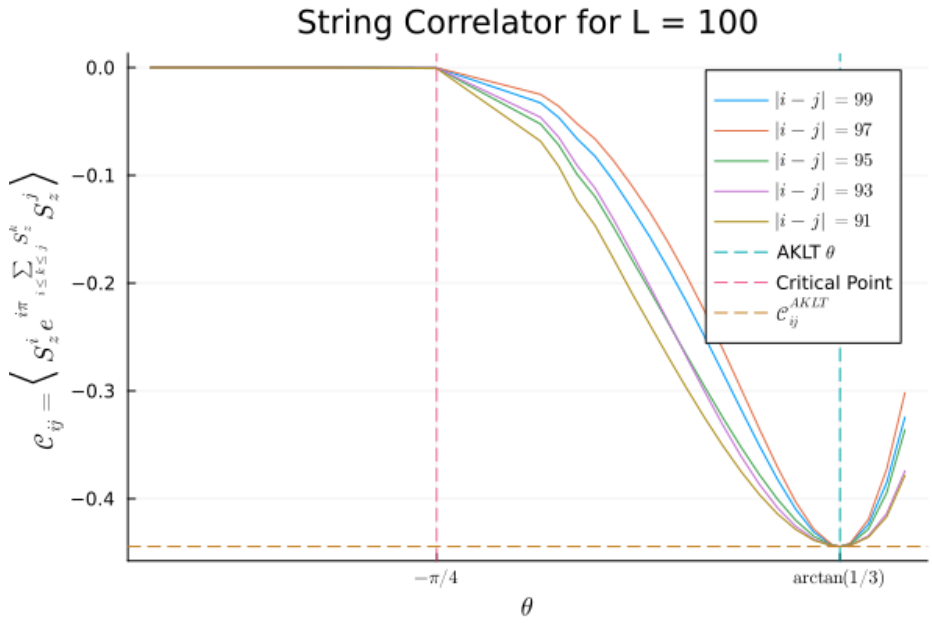

Figure 2.1: String Correlator

We compute the string correlator to identify the critical points. This is given by,

$$\mathcal{C}_{ij}^{\text{string}} := \langle\psi|S_i^z \mathrm{e}^{i\pi\sum_{i<k<j} S_k^z} S_j^z|\psi\rangle \tag{2.2}$$

By varying θ for large lattice separations $|i-j|$, we are able to identify a critical point (see fig 2.1). From the plot, we observe that that the AKLT point is stable against perturbations in θ. Furthermore, the string correlator vanishes at $\theta = -\pi/4$ which we identify as the critical point.

2.3 Central Charge

The von-Neumann entropy at the critical point for a given system size is [1, 3],

$$S_L^{vN}(l) = \frac{c}{6}\ln\left(\frac{2L}{\pi a}\sin\frac{\pi l}{L}\right) + \mathcal{O}(1) = \frac{c}{6}\ln\left(\sin\frac{\pi l}{L}\right) + \mathcal{O}(1), \tag{2.3}$$

where, in the latter equation we have absorbed the constants into $\mathcal{O}(1)$. A special case of this is precisely what we saw in the earlier case with the Ising model where $l = L/2$.

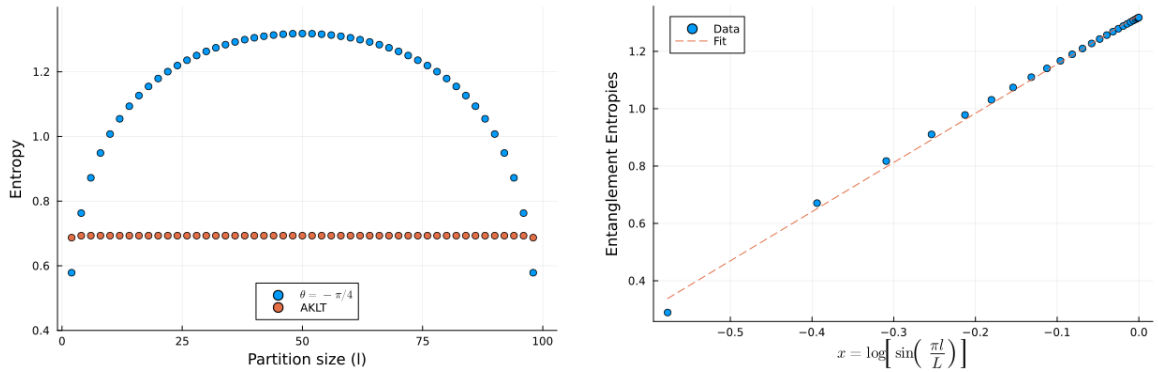

(a) Entropy vs Even Partition Sizes (l)

(b) Entropy vs $\frac{1}{6}\log\left(\sin\left(\frac{\pi l}{L}\right)\right)$

Figure 2.2: Entropy and Central Charge

We plot the entropies at the critical point against even partition sizes (fig 2.2) and observe an area law for the entanglement entropies. Fitting the entropy against the logarithm in (2.3) gives us a value for the central charge $c \approx 1.71$ which is close to the literature value of $c = 1.5$. Since the entropy was found to be symmetric about the half-chain length, the fit was performed by using the mean entanglement entropies between the increasing and decreasing parts in fig 2.2a.

Bibliography

[1] Pasquale Calabrese and John Cardy. Entanglement entropy and quantum field theory. *Journal of Statistical Mechanics: Theory and Experiment*, 2004(06):P06002, jun 2004. URL: https://dx.doi.org/10.1088/1742-5468/2004/06/P06002, doi:10.1088/1742-5468/2004/06/P06002.

[2] Matthew Fishman, Steven R. White, and E. Miles Stoudenmire. The ITensor Software Library for Tensor Network Calculations. *SciPost Phys. Codebases*, page 4, 2022. URL: https://scipost.org/10.21468/SciPostPhysCodeb.4, doi:10.21468/SciPostPhysCodeb.4.

[3] Matteo Rizzi and Markus Schmitt. *MLab Computational Physics - Tensor Networks*. University of Cologne, 2023.